

Hybrid Sliding Mode Control and RNN-Based Strategy for Maximizing Power Extraction in Small Wind Turbines for Electric Vehicles

Khalid Alfuwail*[‡] , Ali Nasir* , Md Shafiullah * , Ayman Abdallah ** 

*Control & Instrumentation Engineering Department, KFUPM, Dhahran, 31261

**Aerospace Engineering Department, KFUPM, Dhahran, 31261

(s202045220@kfupm.edu.sa, ali.nasir@kfupm.edu.sa, shafiullah@kfupm.edu.sa, aymanma@kfupm.edu.sa)

[‡]Khalid Alfuwail; Ali Nasir, 31261, Tel: +966531491639,

Fax: +966-13-860-2965, s202045220@kfupm.edu.sa

Received: 05.02.2025 Accepted: 29.03.2025

Abstract- Advanced technologies like Ram Air Turbines (RATs) are being investigated because of the aviation industry's need for fuel-efficient and alternative renewable energy sources. In situations where power generation is necessary in the event of an emergency involving unmanned aerial vehicles (UAVs), RATs are essential. Optimising the RATs' performance—including power output and operational stability—under variable and unexpected wind conditions is the main obstacle, though. Conventional control techniques frequently don't adjust to these changing conditions. In order to monitor the ideal turbine rotation speed, a sliding mode control rule is developed in the proposed controller. This article emphasises the need of using a recurrent neural network (RNN) to identify unpredictable wind turbine dynamics. Control over maximum power extraction is then made possible by the development of an online update mechanism that provides real-time weight changes for the RNN. Simulation findings show that, even in the presence of significant nonlinearities and system uncertainties, the proposed controller performs 13 times better than a conventional control strategy in monitoring the ideal turbine rotation speed and obtaining the maximum wind output from RATs.

Keywords Wind Power, Maximum wind power extraction, UAVs, Sliding Mode Control, Recurrent Neural Network, Ram air unit air.

1. Introduction

A significant portion of global carbon dioxide emissions are attributed to the aviation industry, which has been identified as the primary emitter of greenhouse gases [1]. The aviation industry has been compelled to discover ways to minimise fuel consumption by the airline sector and alternative power sources to lower the demand for fuel (UAVs) due to severe rules and increased environmental consciousness. Using Ram Air Turbines (RATs) in these vehicles, which harness wind power while in flight, is one method that addresses the issues [2]. This approach is suitable, but it could be ineffective and need more power, which could be problematic for UAVs and other equipment. Therefore, these systems need to perform better so that the UAVs can generate the most power possible to fly for extended periods of time or for other uses where high energy is required rather than low. For instance, in the case of primary power failure,

avionics systems, flight instruments, and auxiliary power units are all essential components that guarantee the UAVs can be manoeuvred, controlled, and securely landed [3].

These methods for improving RAT's performance and boosting its power output have been covered in articles by several academics.

The authors of [4] suggest a passivity-based sliding-mode control (PB-SMC) method for tracking the maximum power point in a Permanent Magnet Synchronous Generator (PMSG). The technique uses passivity theory to enhance system damping and incorporates a sliding-mode control to boost system resilience against uncertainty. Case studies and hardware-in-loop testing verify the study's usefulness and excellence. However, the method ignores real-time flexibility to changing operational conditions in favour of improving damping and durability. Using a doubly fed induction generator (DFIG) for optimal power extraction and improved

fault ride through capability, the second paper [5] designs a robust sliding-mode control for wind energy conversion systems (WECS) using nonlinear perturbation observers. However, it does not specify whether it can be implemented to RATs. The proposed approach combines strong nonlinearities, generator parameter uncertainties, and wind speed unpredictability to generate a perturbation that is evaluated live by a sliding-mode state and perturbation observer (SMSPO). The method removes conventional current regulation loops, simplifying the system.

Multi-variable (SMC) control for UAV engines is introduced in [6], which is an approach that has not yet been proven in this application. The boundary layer approach is used to solve the chattering issue in SMC, and NASA's Commercial Modular Aero-Propulsion System Simulation 40k (C-MAPSS40k) is used to evaluate the control logic. Under various flight situations, the multi-variable SMC's resilience is investigated. The strategy concentrates on improving resilience and decreasing chattering, but it could not adequately handle the requirement for dynamic responsiveness to quickly shifting circumstances and real-time flexibility. Centrifugal angle control, which works well for RATs, is used in another article [7]. The correctness of the model is tested against full-scale wind tunnel testing using computers and moment equilibrium analysis. Increasing spring stiffness and decreasing the blade component's inertia product can boost the rotor's stable rotation speed, according to a sensitivity analysis. However, changing the damping coefficient accelerates the achievement of stability without compromising the stability of the speed.

By combining a PID-control strategy with an integral sliding mode control rule and a (RNN) for simulating the uncertain dynamics of (RATs), this research fills in the gaps found in all previous techniques. This is evidence of the work done by [8], albeit in a new context. Furthermore, MATLAB Simulink was utilised rather than hardware experiments. This combination increases flexibility, guarantees real-time updates, and stabilises the rotating speed. Under various nonlinearities, it maximises power production more effectively. An RNN can achieve the highest power output and maintain system stability in highly nonlinear and rapidly changing situations because to its continuous evaluation and updating capabilities. This can therefore address the issues mostly brought about by PB-SMC and SMSPO-based approaches.

2. Wind Speed Forecasting

2.1. Methodology

The forecasting mechanism that this paper proposes provides real-time wind speed predictions, critical to optimising power generation in RATs on UAVs. By integrating LSTM techniques for predicting wind speed trends and uncertainties in the system, the control system allows turbine operation to adapt in real-time to obtain maximum energy in varying wind conditions. This prediction allows measures to be taken in proactive control and helps to limit power loss caused by sudden shifts in wind, ensuring an increased systematic efficiency and stability. The UAV benefits from continuous

power supply, endurance, and operational reliability due to the forecasting system, making it more an indispensable part of the overall power maximisation design.

The data set contains meteorological reanalysis data for Dhahran, Saudi Arabia. It was downloaded from the Wind Navigator Data Downloaded 3.0.0 on March 22, 2019. Source: NASA/GSFC, Giovanni, user-provided data from AWS True Power LLC Data Information page" MERRA2 MNS"; (Scientist/Program manager) Chad Augustine; and RET Screen. It is situated at 26.5° Latitude and 50° Longitude. It contains hourly meteorological measurements from January 1, 1980, to 2019, as shown in Fig. 1. The following measurements are averaged and recorded:

- wind speed at 50 meters in meters per second
- wind direction at 50 meters measured in degrees
- temperature at 10 and 2 meters above the ground in Celsius degrees
- atmospheric air pressure at ground level measured in kilopascals.

The encoder-decoder LSTM architecture works on tasks like machine translation and text summarization by transforming one sequence into another. This approach deals with variable-length sequences using an encoder to process the input sequence into a fixed-size context vector that captures essential information. Then, the decoder uses this vector to produce the output sequence. The encoder-decoder LSTM has two sets of LSTMs: one for encoding and another for decoding, controlling complicated sequential dependencies. Its keys are the input sequence X, context vector C, and output sequence Y. In Fig. 1, the model is structured architecturally with its data flow.

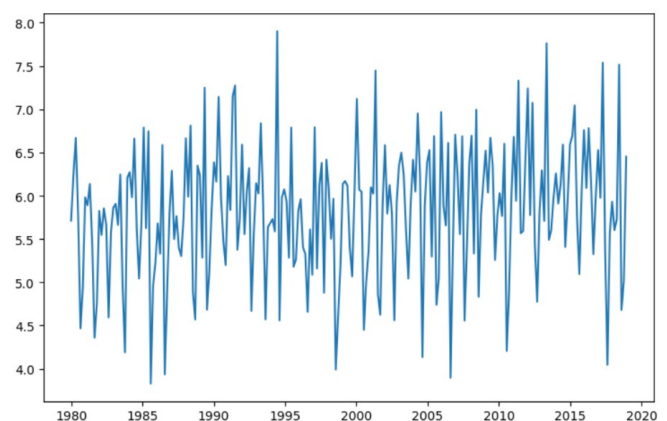


Fig. 1. plot of wind speed distribution at 50 meters.

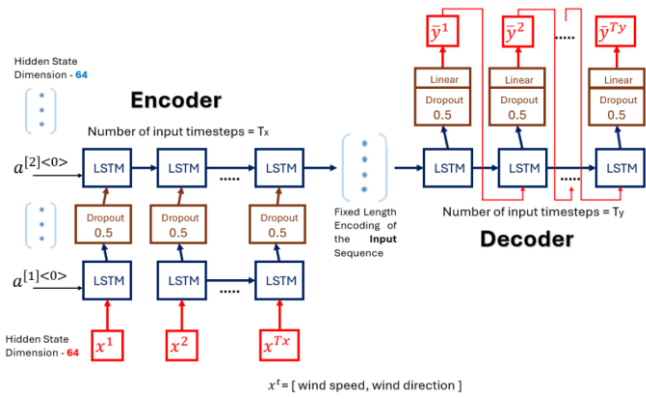


Fig. 2. EnDe-LSTM model architecture for univariate time series data.

2.2. Results

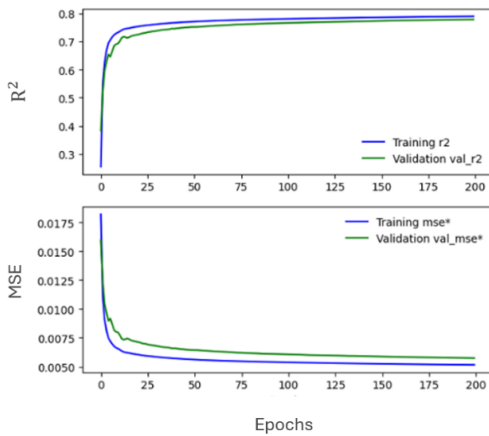


Fig. 3. Training and Validation loss curves over 200 epochs.

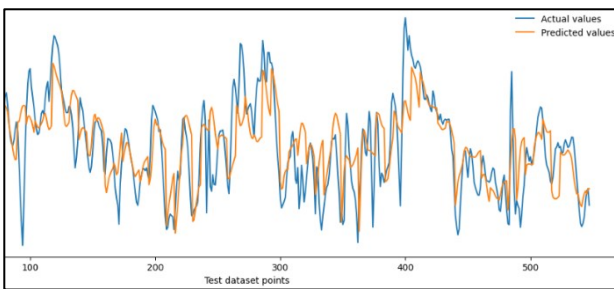


Fig. 4. The prediction of EnDe-LSTM.

The EnDe-LSTM model’s comparative results in Fig. 8 show a better fit at a height level of 50 meters, with lower MSE values indicating better fit. The model’s strength is evident in its decreasing and stable training error and remaining validation errors, proving its generalization well. The model’s R2 score of almost 0.8 also confirms its strength.

As in Fig. The EnDe-LSTM model is a high-accuracy forecasting algorithm for wind speed series prediction, providing 48 predicted time steps and one future time step seven times in every group. Figure 10 shows a strong correlation between predicted and actual values, crucial

for wind energy applications. It’s inaccurate since the focus is on combining it with the sliding mode controller.

3. The Need for The Proposed Approach



Fig. 5. The Hexacopter UAV.

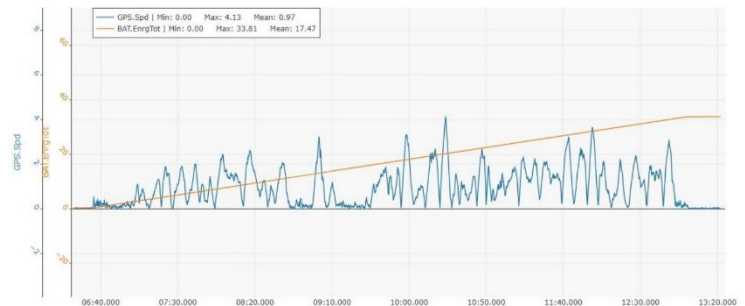


Fig. 6. Speed and Energy consumption vs. Time.

A Hexacopter UAV was experimented with for autonomous flight for around 6 hours and a half, as in Figure 1 and Fig. 2 shows that This experiment measures GPS speed and battery energy consumption over time, with the speed leaping between varied points and reaching its peak speed at 4.13 units, while the energy consumption is seen to rise gradually to a maximum of 33.81 units. The data set that we have here determines the fact that whenever the system is subjected to various loads, power consumption is always increased, which, in turn, underpins the fact that efficient generation of power is highly recommended. Implementing a renewable power generator, like the Ram Air Turbine (RAT), could optimize energy usage, predominantly during peak times, guaranteeing better system performance and sustainability.

2. Methodology

3.1. Ram Air Turbine

Small wind turbines known as ram air turbines (RAT) are employed as power sources in aeroplanes and are coupled to either a hydraulic pump or an electrical generator [9]. Because of the vehicle's speed, they employ ram pressure to create power from the air stream [10]. After a total power failure, the RAT can be manually or automatically deployed. It retracts within the fuselage. Between RAT deployment and power outages, batteries are used. Both the primary engine and the

auxiliary power unit are fuel-burning turbine engines used in modern automobiles. RAT usually operates on the basis of electrical generation, rotational dynamics, and aerodynamic principles. Some of the fundamental equations that can be utilised to explain the RAT are listed below: The wind power that is collected is determined by:

$$R = \frac{1}{2} \rho A^2 v^3 C_p(\lambda, \beta) \quad (1)$$

Air density, turbine radius, wind speed, and the power capture coefficient—which changes with pitch angle and tip speed ratio—are all taken into account in this formula to calculate the power harvested from the wind.

$$\lambda = \frac{\omega_r R}{v} \quad (2)$$

The wind speed, the turbine's radius, and its rotational speed are used to compute the tip speed ratio. The following provides the aerodynamic torque:

$$T_a = \frac{1}{2} \rho R^3 C_p(\lambda, \beta) \frac{v^2}{\lambda} \quad (3)$$

The force that propels the turbine is called aerodynamic torque, and it depends on the power capture coefficient, wind speed, turbine radius, and air density. The ideal rotational speed, which is determined by the ideal tip speed ratio and wind speed, guarantees that the RAT runs at its most efficient point:

$$\omega_{r,opt} = \frac{\lambda_{opt} v}{R} \quad (4)$$

The maximum electrical power output under optimal conditions is given by:

$$P_{g,opt} = C_p n \omega_r^3 \quad (5)$$

The greatest electrical power production attained under ideal circumstances is known as the optimum generator power. Rotational speed, efficiency, and power control gain all play a role. The power control gain, which is described as follows, makes determining the ideal power output easier:

$$k_\infty = \frac{1}{2} \rho R^5 \frac{C_{p,max}}{\lambda_{opt}^3} \quad (6)$$

The air density (ρ), turbine radius (R), and maximum power capture coefficient ($C_{p,max}$) are all included in this equation. By taking into account a number of factors, the computations maximise the RAT system's performance and efficiency in UAVs, guaranteeing excellent electrical system efficiency and maximum power extraction.

3.2. Drive Train Dynamics

The behaviour and operations of several components that transform and transmit power from movement to the generator are known as the drive train dynamics [11]. Two centralised masses make up this system, which is defined by a framework that incorporates torsion and damping. Therefore, when the turbine's rotational speed and the generators are impacted, the mechanical forces and torques are modelled. Examining the

dynamics is essential to improving the performance and durability of wind energy conversion systems [12].

3.3. PMSG Dynamics

In utility-scale wind energy production systems, the Permanent Magnet Synchronous Generator (PMSG) is a dynamically regulated drivetrain technology that streamlines the drive system and boosts efficiency. But according to some experts [13], it has disadvantages, particularly when the mechanical power transfer is eliminated. PMSG is a good option for wind turbine applications because of its increased efficiency, durability, and lack of rotor losses. In order to save costs and improve performance, for instance, a research compared conventional flexible drivetrain topologies to the optimal stiff 3-point mount arrangement [14]. The framework of applying PMSG to the UAV's RAT structure is depicted in Fig. 3, and Fig. 5 provides a detailed view of the controller.

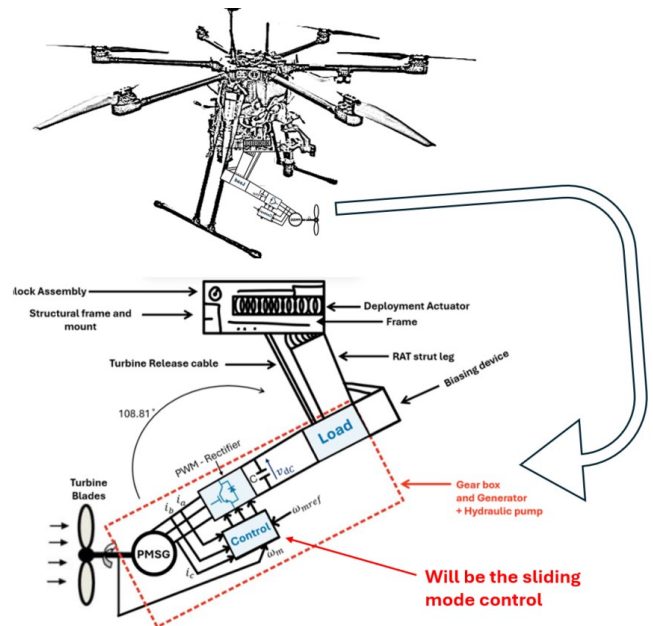


Fig. 7. Structure of a Ram Air Turbine with PMSG.

The rotor speed (ω_r), stator resistance (R_s), and stator inductance (L_s) all have an impact on the stator d-axis and q-axis currents (i_d and i_q) and voltages (u_d and u_q), which describe the dynamics. These are the main equations:

$$\dot{i}_q = -\frac{R_s}{L_s} i_q - n_p n_g \frac{\psi_f}{L_s} \omega_r + \frac{u_q}{L_s} \quad (7)$$

$$\dot{i}_d = -\frac{R_s}{L_s} i_d - n_p n_g \frac{i_q}{L_s} \omega_r + \frac{u_d}{L_s} \quad (8)$$

The permanent magnet flux is denoted by ψ_f , whereas the number of pole pairs and gearbox ratio are denoted by n_p and n_g , respectively. The following provides the electromagnetic torque (T_g):

$$T_g = \frac{3}{2} n_p \psi_f i_q \quad (9)$$

A unity power factor is attained by regulating the d-axis current (i_d) to zero. The equations that have been simplified are:

$$i_q = \frac{R_s}{L_s} i_q - n_p n_g \frac{\psi_f}{L_s} \omega_r + \frac{u_q}{L_s} \quad (10)$$

$$u_d = -n_p n_g \omega_r L_s i_q \quad (11)$$

When these equations are entered into the drive train dynamics equation's time derivative, we get:

$$\dot{\omega}_r = \frac{T_a}{J_d} + \frac{T_g R_s}{L_s J_d} + \frac{B_d}{J_d} \omega_r - \frac{3n_p n_g \psi_f}{2J_d L_s} \omega_r - \frac{3(n_p n_g \psi_f)^2}{2J_d L_s^2} u_q \quad (12)$$

The dynamic equation may be rewritten as follows, taking into account a number of variables like as mistakes, parameter fluctuations, and unmodeled dynamics:

$$\dot{\omega}_r = (a + \Delta a)\omega_r + (b + \Delta b)\omega_r + (c + \Delta c)u_q + \frac{T_a + \hat{T}_a}{J_d}$$

Where a, b, and c are nominal parameters defined as:

$$a = \frac{B_d}{J_d} + \frac{R_s}{L_s} \quad (13)$$

$$b = \frac{3(n_p n_g \psi_f)^2}{2J_d L_s^2} + \frac{B_d R_s}{L_s J_d} \quad (14)$$

$$c = \frac{3n_p n_g \psi_f}{2J_d L_s} \quad (15)$$

By identifying the nominal ranges of T_a , ω_r , and u_q , the lumped uncertainty factor d may be estimated offline. This uncertainty component is mostly produced by variations in unmodeled dynamics, system properties, and aerodynamic torque.

3.4. Neural Network

Wind energy generators' doubtful points (d) are precisely estimated using neural networks (RNNs). Their efficacy stems from their capacity to promptly comprehend intricate disturbances and torque variations, as well as to update weights online [15]. RNNs choose the right input signs to eliminate aggregated uncertainty. Fig. 4 shows the structure of the RNN. The following is a representation of the turbine aerodynamic torque in relation to generator power:

$$P_g = \frac{P_m}{n} \quad (16)$$

These parameters can be used to calculate the lumped uncertainty (d). The RNN's output is an estimate of d , and its inputs are selected as P_g and ω_r .

The input layer's two inputs and outputs are defined as follows:

The measured turbine rotation speed (ω_{rm}) and generator power (P_{gm}) are filtered to remove noise:

$$x_1 = \frac{\omega_r}{1 + 0.05s}; x_2 = \frac{P_{gm}}{1 + 0.05s} \quad (18)$$

The inputs and outputs in the hidden layer are shown as:

$$I_1 = u_i O_j (k - 1) + \sum_{i=1}^6 x_{ij} O_i; \quad (19)$$

$$O_j = g(I_j) = \frac{\exp(I_j)}{\exp(I_j) + \exp(-I_j)} \text{ for } j = 1, 2, \dots, 6 \quad (20)$$

where P_{gm} is the computed generator power and ω_{rm} is the observed RAT rotation speed. To get the lumped uncertainty (d), one neurone in the output layer adds the weighted total of all the output signals from the hidden layer.

$$\hat{d} = \sum_{j=1}^6 \omega_j^T O_j \quad (21)$$

where ω_j denotes the weight between the hidden layer and the O_j is the output of the hidden layer.

3.5. Adjustable Sliding Mode Control Drive Train Dynamics

For instance, system uncertainties and outside disruptions pose a serious threat to power extraction systems' functionality. An adaptive and reliable control approach must be put in place in order to optimise power extraction and maintain the ideal turbine rotation speed. The system uses an integral sliding mode controller to provide a nonlinear robust control approach that accounts for the uncertainties in the system [16]. The suggested controller's structure is depicted in Figure 5. Through online parameter updating, the SMC is designed to monitor the ideal turbine rotation speed and adjust for outside wind disturbances. The sliding mode surface is defined as follows in order to preserve resistance to outside disturbances and accomplish desired closed-loop speed tracking performance:

$$z(t) = \dot{\omega}_r + k_1 \omega_r + k_2 \int_0^t (\omega_r - \omega_{r,opt}) d\tau \quad (22)$$

where k_1 and k_2 are constants, and τ is a dummy variable for integration. Setting $z(t) = 0$, we obtain:

$$\dot{\omega}_r + k_1 \omega_r + k_2 \int_0^t (\omega_r - \omega_{r,opt}) d\tau = 0 \quad (23)$$

The Laplace transformation of this equation results in:

$$\frac{\omega_r}{\omega_{r,opt}} = \frac{k_2}{s^2 + sk_2 + k_2} \quad (24)$$

This transfer function demonstrates that the system can be stabilized by appropriately choosing the coefficients k_1 and k_2 , enabling effective rejection of disturbances and uncertainties. Considering unmodeled dynamics and external

$$x_1 = \omega_r; x_2 = P_g; \quad (17)$$

disturbances, the sliding mode control law is formulated as:

$$u_q = \frac{1}{c}(-k_z(t) - (a + k_1)\dot{\omega}_r - (b + k_2)\omega_r + k_2\omega_{r,opt} - \hat{d}) \quad (25)$$

where k is a positive value for the continuous control gain. The time derivative of $V(t)$ is as follows when the control rule is used in place of the sliding mode surface:

$$\dot{z}(t) = -kz(t) + \hat{\omega}_r + \hat{d} \quad (26)$$

To ensure stability, a Lyapunov function $V(t)$ is defined as:

$$V(t) = \frac{1}{2}z(t)^2 + \frac{1}{2}\hat{\omega}_r^T \Gamma^{-1} \hat{\omega}_r \quad (27)$$

Where the adaptation matrix with positive definite constant Γ is used. The following gives the time derivative of $V(t)$:

$$\dot{V}(t) = -kz^2(t) + \hat{\omega}_r^T \Gamma^{-1} \dot{\omega}_r \quad (28)$$

Since $V(t)$ is negative semi-definite, integrating $V(t)$ over time shows:

$$\int_0^\infty V(t) dt < \infty \quad (29)$$

demonstrating that $z(t)$ and $\hat{\omega}_r(t)$ converge to zero in a finite amount of time, ensuring stable system dynamics and efficient speed tracking performance. Through the gradient of the Lyapunov function, the RNN weights are adjusted online to minimise uncertainty and optimise power extraction and speed monitoring in real-time.

$$\omega_{ij} = \Gamma h(t) O_j \left(-r \frac{\partial V(t)}{\partial \omega_j} \right) \quad (30)$$

The RAT system in UAVs operates at peak efficiency and dependability thanks to the integration of the system's Jacobian $h(t)$ and hidden layer neurones' output O_j to assess lumped uncertainty.

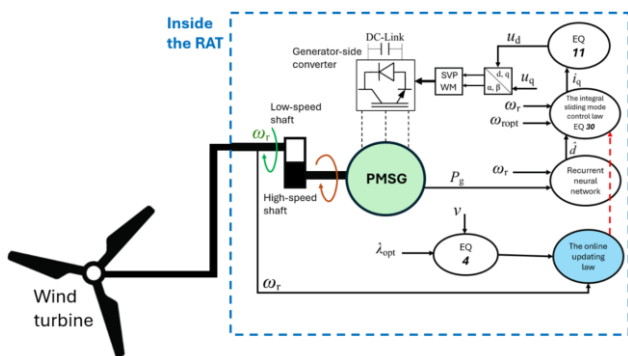


Fig. 8. Structure of the Controller.

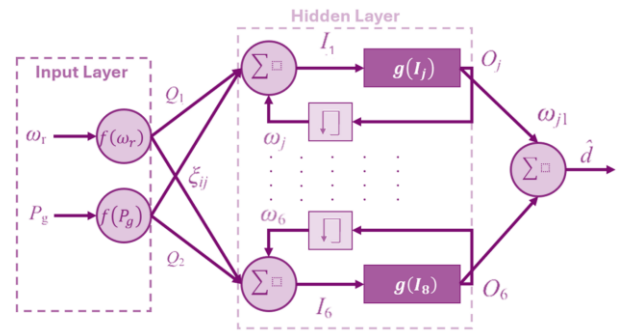


Fig. 9. Structure of the RNN.

4. Results & Discussions

MATLAB R2024a, an Intel Xeon CPU with two virtual CPUs (vCPUs), 13GB of RAM, and Windows 11 were used for the numerical tests. The rated speed was 12 m/s, and the input was the wind speed patterns. The wind speed pattern used in the modelling is shown in Figure 10. The rated wind speed of the turbine is 12 m/s. Over the first ten seconds, the wind speed dropped from 20 m/s to 11 m/s. The wind speed stayed steady at 5 m/s for the following 6 seconds, indicating less wind activity. The wind speed then increased from 12 m/s to 18 m/s at $t=26$ seconds, stabilising at that pace for the rest of the experiment, which is the normal speed they encounter

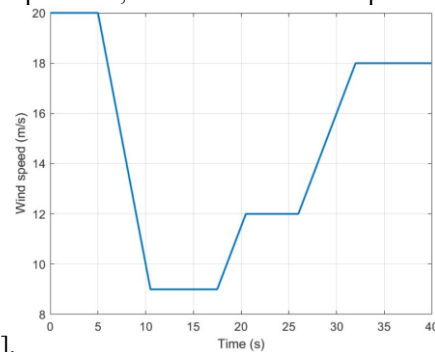


Fig. 10. Wind speed pattern.

As shown in Figure 11(b), the system's rated power output is 0.5 MW. This power is produced with a rated wind speed of 12 m/s. At this speed, the turbine produces less power while maintaining the rated power above it. This is achieved by modifying the blade pitch angle to shade the incoming wind force and maintaining the rotating speed at its optimal level. The ideal tip-speed ratio establishes the ideal rotating speed required to provide the highest power possible at a certain wind speed. The optimal tip-speed ratio for this specific turbine is 7.5, as shown in Fig. 11(a).

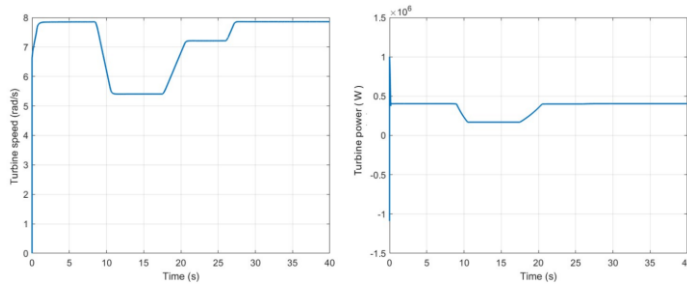


Fig. 11. (a) Turbine Speed (b) Turbine Power

In order to retain the turbine's maximum output at the appropriate wind speed, the turbine speed is modified, as seen in Figure 11(a). The ideal q-axis voltage required to sustain this ideal turbine (generator) speed is determined by the integrated sliding mode controller (SMC) using the optimal and actual rotational rates. One may use the control law to calculate the voltage..

The system utilises the sliding surface, the RNN anticipated lumped uncertainty, and other pertinent data in addition to the natural and ideal turbine rotational rates. This integral sliding mode controller is based on the modelled dynamics of rotational speed.

By linking the turbine's (and therefore the generator's) rotational speed to the turbine and generator torques, this creates the connection between the speed and generator q-axis current. Then, utilising this relationship between current and speed, the integral SMC controller rule is developed to control the speed. The d-axis voltage must be determined in order to maintain the d-axis current at zero. Based on the dq-axis voltage references, the PWM signals driving the three-phase rectifier were generated using Space Vector Pulse Width Modulation (SVPWM). Figure 11(a) makes it clear that the controller can continue to operate at the peak efficiency for any wind speed. As seen in Fig. 11(b), this enabled the system to continue running at its maximum power output for the designated wind speed.

The turbine output increases proportionately to the cube of the wind speed when the wind speed surpasses the required 12 m/s. However, there is a limit to how much electricity the generator can generate. When the wind speed surpasses the rated amount, power shedding uses the pitch angle control mechanism to keep the generated power at this regulated level. The theory states that the turbine's power capture coefficient typically decreases when the blade pitch angle rises while the other turbine parameters stay the same. The blade pitch angle in such cases is shown in Figure 12(a).

To keep the generated power at the designated 400 kW, the blade pitch angle is changed when the wind speed above the rated value, as shown in Fig. 12(c). The pitch angle controller adjusts the blade pitch angle by measuring the power provided by the generated power, comparing it to the rated power, and making the necessary adjustments. There are more turbine variables shown as well.

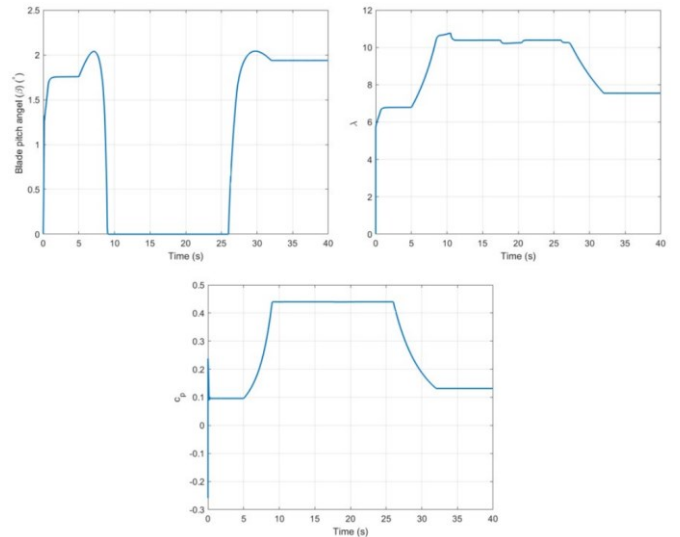


Fig. 12. (a) λ (b) λ (c) β

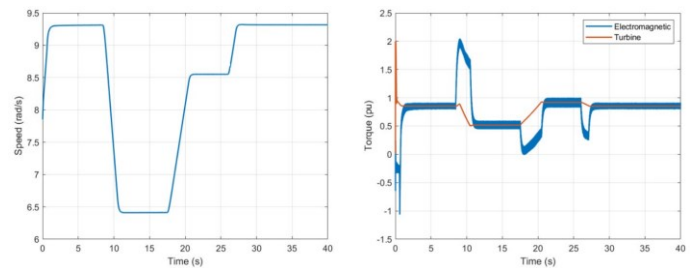


Fig. 13. (a) PMSG rotor speed (b) Turbine and PMSG torque

The PMSG rotor speed and electromagnetic torque are also examined in Figure 13. The rotor's speed closely resembles that of the turbine since it is directly connected to it. Under different wind speeds, a strong connection between electromagnetic and turbine torque is seen in Figure 13(b). The electromagnetic torque, which in turn affects the turbine torque and regulates the rotational dynamics, is directly controlled by the integral SMC. You can see this interaction in Fig. 13(b). The q-axis current is instantly altered by the SMC's control effort, which also varies the electromagnetic torque to preserve the intended rotating speed.

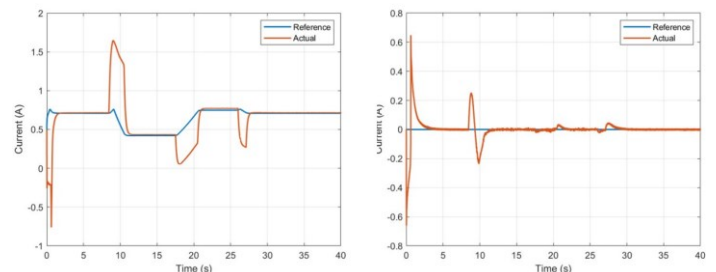


Fig. 14. (a) d-axis current control (b) q-axis current control

The d-axis and q-axis current controller responses are seen in Fig. 14. In Fig. 14(a), the d-axis current is managed until it reaches the desired value of zero. The q-axis current is also investigated in Fig. 14(b), which shows both the reference generated by the speed controller loop based on the

electromagnetic torque requirement and the actual q-axis current from the integrated SMC-controlled system. It should be noted that while the rotational speed dynamics indirectly affect the q-axis current reference value shown in the picture, the SMC does not use it. Here, the difference between the PI-controlled cascaded control approach and the integral SMC-based control technique is illustrated. As a result, the variations between the reference and actual q-axis current shown in the figure are just meant to serve as examples.

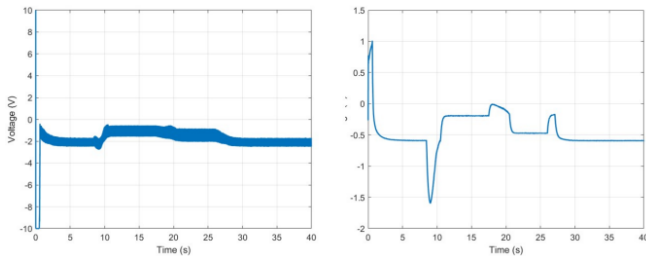


Fig. 15. (a) d-axis voltage (b) q-axis voltage.

By generating PWM switching signals based on those reference voltage values, the current controllers were able to regulate the rectifier by creating dq-axis voltages.

Furthermore, the RNN-calculated lumped uncertainty in Fig. 16 is examined. The RNN is used to estimate this cumulative uncertainty. Since it is challenging to determine this quantity precisely in practice, RNN estimate is necessary. This quantity is based on the measured generator power and rotational speed. Changes in neural weights help the RNN estimate lumped uncertainty accurately. The figure clearly shows that the RNN estimation of the aggregated uncertainty gets close to the true value if enough time is allowed.

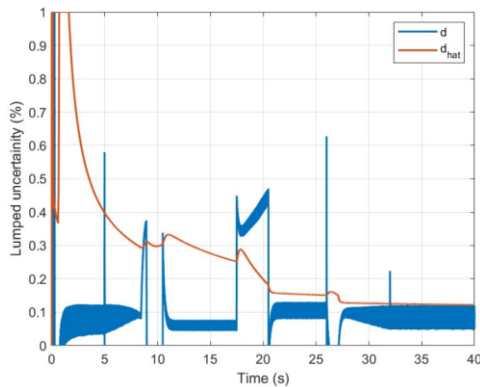


Fig. 16. Lumped uncertainty.

5. Conclusion

In order to manage and optimise the installation of wind energy conversion systems in Ram Air Turbines (RATs), this study combines Sliding Mode Control (SMC) with uncertainty estimates based on Recurrent Neural Networks (RNNs). Even in the face of outside disruptions and system uncertainties, the SMC technique maximises output by stabilising the turbine's rotational speed. Furthermore, the RNN models and updates the uncertain dynamics continually, producing precise estimates that improve the resilience of the control system.

The system produces 1500 kW, or about 13 times more than the typical RATs, which in some situations only generate 110 kW, by optimising power production in reaction to wind conditions, which impact the turbine speed and torque [18].

The control system will eventually need to be implemented as hardware in order to be validated in real application areas. This action will improve the UAV's performance and dependability even further. Power generation will therefore be effective in a variety of operational situations, which are common with UAVs. Additionally, hardware implementation will enable assessment under various situations and the investigation of other environmental factors, providing thorough insights into its potential for wider usage in wind energy conversion systems. For instance, the RAT system may be simulated by a smaller wind turbine equipped with a Permanent Magnet Synchronous Generator (PMSG), which is managed by an STM32 microprocessor that uses the Sliding Mode Control (SMC) algorithm. Real-time uncertainty estimate is handled by an RNN model on a DSP or Nvidia Jetson, which maximises power production and stability under a range of wind conditions.

Acknowledgements

The author(s) would like to acknowledge the research supported by the Interdisciplinary Research Center for Aviation & Space Exploration (IRC-ASE) at King Fahd University of Petroleum & Minerals (KFUPM). The Authors also acknowledge the flight data obtained from the project done by the team UAS2030 (a team that represents the university annually in the global SUAS Competition).

References

- [1] G. Buticchi, P. Wheeler, and D. Boroyevich, "The more-electric aircraft and beyond," *Proceedings of the IEEE*, vol. 111, no. 4, pp. 356–370, 2023.
- [2] T. Moustafa and W. Moreno, "Ram air and wind energy harvesting survey for electrical vehicles and transportation," in *SoutheastCon 2017*, 2017, pp. 1–7.
- [3] M. Hovanec, P. Korba, P. Šváb, R. Baláž, and M. Golisová, "Auxiliary power unit - system essentials," in *2019 New Trends in Aviation Development (NTAD)*, 2019, pp. 73–76.
- [4] B. Yang, T. Yu, H. Shu, Y. Zhang, J. Chen, Y. Sang, and L. Jiang, "Passivity-based sliding-mode control design for optimal power extraction of a pmsg based variable speed wind turbine," *Renewable Energy*, vol. 119, pp. 577–589, 2018.
[Online]. Available: <https://www.sciencedirect.com/science/article/pii/S096014811731251X>
- [5] B. Yang, T. Yu, H. Shu, J. Dong, and L. Jiang, "Robust sliding mode control of wind energy conversion systems for optimal power extraction via nonlinear perturbation observers," *Applied Energy*, vol. 210, pp. 711–723, 2018.
[Online]. Available: <https://www.sciencedirect.com/science/article/pii/S0306261917310486>

- [6] S. Sangwian, "Multivariable sliding mode control design for aircraft engines," Ph.D. dissertation, Cleveland State University, 2011.
- [7] X. Tianxiang, L. Yueliang, and Z. Dongyu, "Study on the rotation speed control method for ram air turbine system," in CSAA/IET International Conference on Aircraft Utility Systems (AUS 2018). Institution of Engineering and Technology, 2018.
- [8] X. Yin, Z. Jiang, and L. Pan, "Recurrent neural network based adaptive integral sliding mode power maximization control for wind power systems," *Renewable Energy*, vol. 145, pp. 1149–1157, 2020. [Online]. Available: <https://www.sciencedirect.com/science/article/pii/S0960148118315520>
- [9] X. Zhao, L. Wang, and M. Zhou, "Comparative analysis of ram air turbine system for large civil aircraft," in CSAA/IET International Conference on Aircraft Utility Systems (AUS 2022), vol. 2022. IET, 2022, pp. 429–434.
- [10] M. M. M. Saad, S. Mohd, M. F. Zulkafli, N. A. Samiran, and D. H. Didane, "Cfd simulation study on the performance of a modified ram air turbine (rat) for power generation in aircrafts," *Fluids*, vol. 6, no. 11, 2021. [Online]. Available: <https://www.mdpi.com/2311-5521/6/11/391>
- [11] D. Jiménez-Santín, M. Cerrada, J. Enríquez-Zárate, D. Cabrera, and R.- V. Sánchez, "Drive-train third stage-based simplified dynamic modelling of a wind turbine oriented to vibration analysis," in 2023 IEEE Seventh Ecuador Technical Chapters Meeting (ECTM), 2023, pp. 1–6.
- [12] Q. Lai, C. Shen, and D. Li, "Dynamic modeling and stability analysis for repeated lvr process of wind turbine based on switched system theory," 2024. [Online]. Available: <https://arxiv.org/abs/2404.01155>
- [13] Y. Yang, D. Liang, F. Zhao, Y. Li, S. Yin, and M. Yang, "Reliability evaluation of wind-storage power generation system considering fatigue failure of wind turbine gearbox," in 2022 IEEE 5th International Electrical and Energy Conference (CIEEC), 2022, pp. 3184–3189.
- [14] S.-H. Park, C.-J. Kim, and Y. Kang, "Evaluation of the supporting mounts of a three-in-one electric drive unit using a hybrid simulation model," *Machines*, vol. 11, no. 11, 2023. [Online]. Available: <https://www.mdpi.com/2075-1702/11/11/1026>
- [15] G. Kothapalli, "An analogue recurrent neural network for trajectory learning and other industrial applications," in INDIN '05. 2005 3rd IEEE International Conference on Industrial Informatics, 2005., 2005, pp. 462–467.
- [16] W. M. E. Ahmed M. Elmogy, Amany Sarhan, "An adaptive real-time third order sliding mode control for nonlinear systems," *Computers, Materials & Continua*, vol. 72, no. 3, pp. 5629–5641, 2022. [Online]. Available: <http://www.techscience.com/cmcc/v72n3/47465>
- [17] J. Inoue and K. Sato, "Wind speed measurement by an inexpensive and lightweight thermal anemometer on a small uav," *Drones*, vol. 6, no. 10, 2022. [Online]. Available: <https://www.mdpi.com/2504-446X/6/10/289>
- [18] Innovative Ram Air Turbine for Airborne Power Generation, ser. Turbo Expo: Power for Land, Sea, and Air, vol. Volume 8: Microturbines, Turbochargers and Small Turbomachines; Steam Turbines, 06 2015. [Online]. Available: <https://doi.org/10.1115/GT2015-4343>.